HHS Public Access

Author manuscript

Biomaterials. Author manuscript; available in PMC 2016 December 01.

Published in final edited form as:

Biomaterials. 2015 December ; 72: 74–89. doi:10.1016/j.biomaterials.2015.08.048.

Hyaluronic acid-decorated dual responsive nanoparticles of Pluronic F127, PLGA, and chitosan for targeted co-delivery of doxorubicin and irinotecan to eliminate cancer stem-like cells

Hai Wang[a,b,c], **Pranay Agarwal**[a,b], **Shuting Zhao**[a,b], **Ronald X. Xu**[a,b], **Jianhua Yu**[c,d], **Xiongbin Lu**[e], and **Xiaoming He**[a,b,c,*]

[a]Department of Biomedical Engineering, The Ohio State University, Columbus, OH 43210, USA

[b]Davis Heart and Lung Research Institute, The Ohio State University, Columbus, OH 43210, USA

[c]Comprehensive Cancer Center, The Ohio State University, Columbus, OH 43210, USA

[d]Division of Hematology, The Ohio State University, Columbus, OH 43210, USA

[e]Department of Cancer Biology, The University of Texas MD Anderson Cancer Center, Houston, TX 77030, USA

Abstract

Dual responsive nanoparticles are developed for co-delivery of multiple anticancer drugs to target the drug resistance mechanisms of cancer stem-like cells (CSCs). The nanoparticles consist of four polymers approved by the Food and Drug Administration (FDA) for medical use: Poly(D,L-lactide-co-glycolide) (PLGA), Pluronic F127 (PF127), chitosan, and hyaluronic acid (HA). By combining PLGA and PF127 together, more stable and uniform-sized nanoparticles can be obtained than using PLGA or PF127 alone. The HA is used for not only actively targeting CSCs to reduce their drug resistance due to dormancy (i.e., slow metabolism), but also replacing the commonly used poly(vinyl alcohol) as a stabilizing agent to synthesize the nanoparticles using the double-emulsion approach and to allow for acidic pH-triggered drug release and thermal responsiveness. Besides minimizing drug efflux from CSCs, the nanoparticles encapsulated with doxorubicin hydrochloride (DOX, hydrophilic) and irinotecan (CPT, hydrophobic) to inhibit the activity of topoisomerases II and I, respectively, can fight against the CSC drug resistance associated with their enhanced DNA repair and anti-apoptosis. Ultimately, the two drugs-laden nanoparticles can be used to efficiently destroy the CSCs both *in vitro* and *in vivo* with up to ~500 times of enhancement compared to the simple mixture of the two drugs.

Keywords

cancer stem-like cell; drug resistance; CD44; co-delivery; topoisomerase

*Correspondence should be addressed to: Department of Biomedical Engineering, The Ohio State University, 1080 Carmack Road, Columbus, OH, Phone: 1 (614) 247-8759, Fax: 1 (614) 292-7301, he.429@osu.edu.

1. Introduction

Cancer stem-like cells (CSCs) are rare subpopulations of cancer cells that are highly tumorigenic (i.e., highly capable of initiating and/or reinitiating tumor growth). There is mounting evidence that the CSCs are responsible for cancer metastasis and tumor recurrence or relapse associated with conventional chemo, radio, and hormone therapies [1,2]. As a result of the failure to eliminate tumor relapse in many cancer patients, CSCs have attracted a great deal of attention in the field of oncology in the past ~10 years. For chemotherapy, several characteristics of CSCs contribute to their drug resistance including overexpressed drug efflux pumps, enhanced DNA repair, overexpression of anti-apoptotic proteins, and dormancy (i.e., slow metabolism) [3–5]. Therefore, rational approaches to target the mechanisms of drug resistance of CSCs are emerging as a novel strategy to improve the clinical outcome of chemotherapy for cancer treatment [6,7].

One such approach is to use nanoparticles to overcome drug resistance in cancer [8,9]. A considerable number of studies have been reported on delivering chemotherapeutic drugs using nanoparticles to enhance their anti-tumor capacity while minimizing their side effects [10–12]. Nanoparticles with a size ranging over 10–100 nm have been reported to be effective for passively targeting tumors through the enhanced permeability and retention (EPR) effect of the vasculature in tumors, compared to normal tissues [13]. Along with the EPR effect, nanoparticles with active targeting moieties and environmental stimuli-responsiveness have attracted more and more attention for cell and/or tissue-specific drug delivery [11,12,14,15]. By delivering more chemotherapeutic drugs into tumor and cancer cells, nanoparticles can help to combat drug resistance. Moreover, nanoparticles can be used to circumvent the mechanisms of drug resistance. For example, the drug efflux pumps across the plasma membrane of drug resistant cancer cells can rapidly evacuate free drug out of the cells because free drug enters the cells through passive diffusion across the plasma membrane with close proximity to the pumps. By contrast, nanoparticles are usually taken up by cells via endocytosis to release drug into the inner cytosol away from the efflux pumps [16–18].

Another approach for overcoming drug resistance is the concurrent use of two or more chemotherapeutic drugs with different anti-tumor mechanisms [19]. As aforementioned, CSCs have enhanced capability of DNA repair and overexpression of anti-apoptotic proteins, both of which contribute to their drug resistance. DNA topoisomerases I and II are enzymes that can modify negatively and positively supercoiled DNA circles through concerted breaking and rejoining of the DNA strands. Topoisomerases have been shown to increase the transcription rates, help to repair DNA, and facilitate the production of anti-apoptotic proteins [20]. Therefore, it is reasonable to fight against the CSC drug resistance by inhibiting both topoisomerases I and II with appropriate drugs [21,22]. However, the current practice of simply using multiple free drugs with no control of their delivery and release is far from being optimal for utilizing the anticancer capacity of the drugs. This is due to the vastly differing physiochemical and pharmacokinetic properties of different drugs including solubility, biodistribution, half-life in blood circulation, and membrane transport properties, which could lead to completely different doses of the multiple drugs in tumor from that administered initially. This deficiency makes dosing and scheduling an optimal

regimen of administering the multiple free anticancer agents *in vivo* extremely difficult if not impossible [9,23]. Therefore, it is desired to co-deliver the drugs so that they could arrive at the tumor site together at the similar dose ratio to that initially administered.

In this study, we developed a "green" approach to prepare dual-responsive nanoparticles that are loaded with two topoisomerase-inhibiting anticancer drugs and capable of actively targeting CSCs without the need of chemical reaction to break or form covalent bonds. This was achieved by using four polymers that are approved by the FDA for medical use: PLGA, Pluronic F127 (PF127 with and without chitosan modification), chitosan, and hyaluronic acid (HA). HA was used as a stabilizer to replace the conventionally used poly (vinyl alcohol) (PVA) and as a moiety to decorate the nanoparticle surface for actively targeting the variant CD44 receptor commonly overexpressed on many types of CSCs [24–26]. PF127, a nonionic triblock copolymer of poly (propylene glycol) (PPG) and poly (ethylene glycol) (PEG), was used to achieve thermal responsiveness [27–29]. Two drugs, the hydrophilic doxorubicin hydrochloride (DOX) and hydrophobic irinotecan (CPT), were incorporated into the nanoparticles using an improved double-emulsion method. We tested this multifunctional nanoparticles *in vitro* using 3D cultured mammospheres (i.e., breast cancer cell spheroids enriched with CSCs) and prostaspheres (i.e., prostate cancer cell spheroids enriched with CSCs) and *in vivo* with orthotopic triple-negative human mammary tumors grown in the fat pad of the mammary gland of nude mice. The targeted co-delivery system was found to significantly improve the efficacy of eliminating the CSCs both *in vitro* and *in vivo*, leading to much enhanced destruction of orthotopic triple-negative human mammary tumors with no evident systemic toxicity.

2. Materials and methods

2.1 Materials

PLGA (lactide:glycolide: 75:25, M_w: 4,000–15,000) and Pluronic F127 (PF127) were purchased from Sigma (St. Louis, MO, USA). Hyaluronic acid (HA, M_w: 66–90 kDa) was purchased from Lifecore Biomedical (Chaska, MN, USA). Polyvinyl Alcohol (PVA, M_w: 100 kDa) was purchased from Fisher Scientific (Pittsburgh, PA, USA). Chitosan oligosaccharide of pharmaceutical grade (M_w: 1.2 kDa, 95% deacetylation) was purchased from Zhejiang Golden Shell Biochemical Co. Ltd (Zhejiang, China). The WST-1 cell proliferation reagent was purchased from Roche Diagnostics (Mannheim, Germany). Fetal bovine serum (FBS) and penicillin/streptomycin were purchased from Invitrogen (Carlsbad, CA, USA). The F-12K and DMEM cell culture media were purchased from ATCC (Manassas, VA, USA). Doxorubicin was purchased from LC laboratories (Woburn, MA, USA). Irinotecan was purchased from Selleck Chemicals (Houston, TX, USA). All other chemicals were purchased from Sigma unless specifically mentioned otherwise.

2.2 Preparation of chitosan-modified PF127 (chitosan-PF127)

The chitosan-PF127 was prepared using a previously reported procedure [28,29]. Briefly, a total of 30 ml of PF127 solution (26 mM in benzene) was added dropwise into 30 ml solution of 4-nitrophenyl chloroformate (4-NPC) (160 mM in benzene) and the mixture was stirred for 3 h in N_2 atmosphere at room temperature to activate PF127. The activated

polymer was then precipitated and filtered in excess (ice-cold) diethyl ether for three times and dried under vacuum overnight. To synthesize chitosan-PF127, 10 ml chitosan solution (200 mg/ml, in DI water) was added dropwise into 10 ml activated PF127 solution (400 mg/ml, in DI water). After stirring for 12 h, this mixture was dialyzed (MWCO: 7 kDa) against DI water for 24 h. Lastly, the polymer was freeze-dried for 48 h to remove water for further use.

2.3 Preparation of nanoparticles

The PLGA nanoparticles and PF127 nanoparticles were prepared using a double emulsion (water in oil in water or W/O/W) method with slight modification [30]. Briefly, 10 mg of PLGA was dissolved in 2 ml of dichloromethane and the PLGA solution together with 0.4 ml of DI water was transferred into a centrifuge tube where the two immiscible solutions were emulsified by sonication for 1 min using a Branson 450 sonifier. Afterward, this initial emulsion and 4 ml of 2% polyvinyl alcohol (PVA) solution (in DI water) were emulsified by sonication for 2 min to obtain the double emulsion that was further processed by slowly dropping into 6 ml of 0.6% PVA (in DI water) and stirred for 10 min at room temperature. After rotary evaporation of the double emulsion to remove organic solvent, the PLGA Nanoparticles were collected by centrifugation at 1,620 g for 10 min at room temperature and washed twice with DI water. The PF127 Nanoparticles were prepared in the same way as the PLGA Nanoparticles except that they were washed by dialysis (MWCO: 50 kDa) against DI water because they could not be collected by centrifugation.

To prepare PF127-PLGA (PFP) and HAC-PFP (with or without drug) nanoparticles, 10 mg of PLGA together with a desired (to be specified later for different nanoparticles) amount CPT and PF127 was dissolved in 2 ml of dichloromethane. After adding 0.4 ml DI water either with or without DOX, the immiscible solutions were emulsified by sonication for 1 min. Then, this first emulsion and 4 ml of chitosan-PF127 (and HA for HAC-PFP Nanoparticles) solution (in DI water) were emulsified by sonication for 2 min. After rotary evaporation to remove organic solvent, the nanoparticles were collected by centrifugation at 1,620 g for 10 min at room temperature and washed twice with DI water.

2.4 Characterization of nanoparticles

The morphology of nanoparticles was characterized using both transmission (TEM) and scanning (SEM) electron microscopy. For TEM study, the nanoparticles were negatively stained with uranyl acetate solution (2%, w/w) and examined using an FEI (Moorestown, NJ, USA) Tecnai G2 Spirit transmission electron microscope. SEM experiments were conducted by depositing 10 μL of aqueous suspension of the nanoparticles on a freshly cleaved mica grid and allowing them to dry for 60 minutes in air. A thin film of Au was then sputtered onto the nanoparticles on the substrate. Samples were imaged with an FEI NOVA nano400 scanning electron microscope.

The nanoparticle size (diameter, nm), polydispersity index (PDI), and surface charge (or zeta potential) were determined using a Brookhaven (Holtsville, NY, USA) 90 Plus/BI-MAS dynamic light scattering (DLS) instrument by dispersing the nanoparticles at 1 mg/ml in DI water. When measuring the size and zeta potential at 37 °C, the samples were incubated for

10 min in the instrument with its sample holder set at 37 °C to ensure the temperature reached equilibrium in the sample before starting the measurement.

Successful preparation of the various nanoparticles was further confirmed by using Fourier transform infrared spectrometry (FTIR) using a Perkin Elmer (Waltham, MA, USA) Spectrum 100 FTIR spectrometer, for which the various materials/nanoparticles were dissolved in dichloromethane, pipetted onto the potassium bromide FTIR sample holder, and dried at room temperature to form a thin layer for examination.

2.5 Drug encapsulation efficiency and in vitro release

Encapsulation efficiency (EE) of drugs using the Nanoparticles was calculated by the following equation:

$$\mathrm{EE}=\mathrm{A}/\mathrm{B}\times 100\% \quad (1)$$

where A represents the amount of drug retained in nanoparticles and B is the initial amount of drug fed for encapsulation. The amount of DOX and CPT in the nanoparticles was determined using a Beckman Coulter (Indianapolis, IN, USA) DU 800 UV-Vis spectrophotometer based on their absorbance at 483.5 and 370.0 nm, respectively.

For *in vitro* drug release study, drug-laden nanoparticles (20–30 mg) were reconstituted in PBS (5 ml, pH 5 or 7.4) and transferred into dialysis bags (MWCO: 20 kDa) that were placed in 30 ml of the same PBS at 37 °C and stirred at 220 g using a mini-stir bar. At appropriate time points, 100 μl of the dialysate was collected and the dialysate replenished with the same amount of fresh PBS. The concentration of the released DOX and CPT in the removed dialysate was determined using UV-Vis spectrophotometer based on their absorbance.

2.6 Culture of cancer cells and cancer stem-like cells (CSCs)

Human prostate adenocarcinoma PC-3 cancer cells (ATCC, Manassas, VA, USA) were cultured in F-12K medium supplemented with 10% FBS and 1% penicillin/streptomycin at 37 °C in a humidified 5% CO_2 incubator. Human breast adenocarcinoma MDA-MB-231 cancer cells (ATCC) were cultured in DMEM supplemented with 10% FBS and 1% penicillin/streptomycin at 37 °C in a humidified 5% CO_2 incubator.

To obtain prostaspheres and mammospheres enriched with CSCs, the well-established suspension culture was used [31,32]. Briefly, detached single cancer cells (PC-3 and MDA-MB-231 cells for prostaspheres and mammospheres, respectively) were cultured in 24-well ultralow attachment plates (Corning, Lowell, MA, USA) at a density of 20,000 cells/ml in 1 ml CSC medium consisting of serum-free DMEM/F12-K supplemented with 5 μg/ml insulin, 20 ng/ml epidermal growth factor (EGF), 20 ng/ml basic fibroblast growth factor (bFGF), 1×B27 (Invitrogen), and 0.4% (w/v) bovine serum albumin (BSA). After 10 days, the prostaspheres or mammospheres were collected for further experimental use.

2.7 Cellular uptake and intracellular distribution of nanoparticles

To study cellular uptake of drugs/nanoparticles and their intracellular distribution, different drug formulations were cultured with the prostaspheres/mammospheres for 3 h. To obtain a homogeneous solution/suspension of free CPT, we mixed the sample of free CPT in medium for 30 min in an ultrasonic cleaner. No other solvent was used to help with dissolving the free CPT since the goal of this study is to show that encapsulation of CPT in nanoparticle could improve its aqueous solubility and bioavailability to cells. The cells were further treated with medium containing 75 nM LysoTracker Green DND-99 to stain late endosomes/lysosomes. Finally, the prostaspheres/mammospheres were mounted onto a glass slide with anti-fade mounting medium from Vector Laboratories (Burlingame, CA, USA) for further examination using a Zeiss (Oberkochen, Germany) Axio Observer.Z1 microscope.

To quantify cellular uptake of different drug formulations using flow cytometry, the prostaspheres/mammospheres were incubated with medium containing different drug formulations for 3 h, washed twice with 37 °C PBS, detached using trypsin/ethylenediaminetetraacetic acid (EDTA), and further dissociated by gentle pipetting for analysis using a BD (Franklin Lakes, NJ, USA) LSR-II flow cytometer and Diva software.

2.8 Cancer destruction studies with the 3D prostasphere and mammosphere model

For cancer destruction study, the 3D prostaspheres/mammospheres (enriched with CSCs) obtained after 10-day suspension culture in the CSC medium in 24-well plates were further incubated for 10 days in CSC medium containing blank nanoparticles, free DOX, free DOX and free CPT (dissolved in medium with the ultrasonic method mentioned in the previous section) (DOX & CPT), DOX encapsulated in HAC-PFP nanoparticles (HAC-PFP-D), DOX and CPT encapsulated in PFP nanoparticles (PFP-DC), and DOX and CPT encapsulated in HAC-PFP nanoparticles (HAC-PFP-DC). The total drug content in all the groups was kept to be the same except the blank nanoparticle group with 0 drug content. To determine cell viability on day 10, fresh CSC medium with 10% Roche (Mannheim, Germany) WST-1 reagent was added to each well and incubated for 4 h at 37 °C and the absorbance at 450 nm was quantified using a Perkin Elmer VICTOR™ X4 multilabel plate reader. Cell viability was calculated as the ratio of the cell number determined for each group to that of control with no treatment. Moreover, phase images of the prostaspheres/mammospheres were taken on different days during the 10-day incubation to quantify the time-dependent size (area) of the prostaspheres/mammospheres for the various treatments.

2.9 Cell cycle analysis

Flow cytometry was used to analyze cell cycle distribution. To determine the effect of different drug formulations on the cell cycle, prostaspheres enriched with CSCs were treated with free DOX, free CPT (dissolved with 0.5% DMSO to ensure its bioavailability for this specific experiment), and HAC-PFP encapsulated with DOX and CPT (HAC-PFP-DC) for 48 h. The prostaspheres were then detached and disassociated as aforementioned and the disassociated single cells were fixed for 30 min in an ice-cold 70% ethanol solution containing ribonuclease (RNase, 2 mg/ml). Cells were then washed in PBS and stained with propidium iodide (PI) for 10 min. The PI-elicited fluorescence in the single cells was

measured using flow cytometry as aforementioned. The data were analyzed using the BD ModFit software.

2.10 Animals and orthotopic xenograft of human breast tumors

Athymic male NU/NU nude mice of 6-week old were purchased from Charles River (Wilmington, MA, USA) and maintained on a 16:8 h light-dark cycle. All procedures for animal use were approved by the Institutional Animal Care and Use Committee (IACUC) at The Ohio State University and all efforts were made to minimize animal suffering. To obtain xenograft of human prostate tumor in the nude mice, detached mammospheres cells were suspended at 2×10^5 cells/ml in a mixture (1:1) of 1× PBS and matrigel. A total of 20, 000 cells in 100 μl of the mixture were injected subcutaneously at the fat pad of mammary gland of nude mice of each 7-week-old mouse.

2.11 In vivo antitumor efficacy and systemic toxicity

After tumors reached ~5 mm in diameter, mice were treated with 100 μl saline or HAC-PFP nanoparticles, DOX&CPT (DOX: 1.5 mg/kg, CPT: 1.5 mg/kg body weight dissolved with 10 μl ethanol before adding into 100 μl saline), HAC-PFP-D nanoparticles (DOX: 3 mg/kg body weight), PFP-DC nanoparticles (DOX: 1.5 mg/kg, CPT: 1.5 mg/kg body weight), and HAC-PFP-DC nanoparticles (DOX: 1.5 mg/kg, CPT: 1.5 mg/kg body weight) at day 1, 7, and 14. Tumor growth was monitored every two days. The tumor volume (V) was calculated as: $V = (L \times W^2)/2$, where L is long diameter and W is short diameter determined using a caliper. The mice were euthanized at day 30 after the drug injection. Tumors, livers, lungs, hearts, spleens, and kidneys were collected, formalin fixed, paraffin embedded, and haematoxylin&eosin (H&E) stained for further histological analysis.

2.12 CD44, CD133, annexin V, and propidium iodide (PI) staining

For immunohistochemical staining with the two CSC surface receptor markers (CD44 and CD133), tumors were collected and put in frozen with the Tissue-Tek (Sakura Finetek, Torrance, CA, USA) O.C.T. Compound and Cryomold at −80 °C for 24 h. The tumors were then cut into slices of 10 μm thick using a cryo-microtome and transferred onto microscope slides. For CD133 staining, the slides were washed with FcR blocking reagent and incubated with PE labeled CD133 (1:11 dilution, Miltenyi Biotec, Auburn, CA, USA) for 30 min in the dark at 4 °C. For CD44 stating, the slides were incubated in 3% BSA in 1× PBST (1× PBS and 0.05% Tween 20) at room temperature for 1 h to block potential non-specific binding, followed by overnight incubation at 4 °C with primary antibodies CD44 (1:40 dilution, Abcam, Cambridge, MA, USA). The samples were then washed 3 times and incubated in dark at room temperature for 1 h with secondary antibodies (Abcam, FITC labeled) diluted in 3% BSA in 1× PBST (1:50 dilution). Afterward, the samples were washed and further stained for nuclei using Hoechst 33342 (5 μM) for further examination using an Olympus FV1000 confocal microscope.

For annexin V and PI staining, the tumors were cut into slices of 20 μm thick using same method mentioned above. The slides were washed with PBS for three times, and transferred to 1 × binding buffer (0.1 M HEPES, pH 7.4, 1.4 M NaCl, 25 mM $CaCl_2$, diluted to 1 × prior to use) with Annexin V (BD, San Jose, CA, USA) and PI (BD, San Jose, CA, USA).

Then, the slides were incubated with binding buffer for 15 min at room temperature in dark. The samples were then washed and further stained for nuclei using Hoechst 33342 (5 μM) for further examination using an Olympus FV1000 confocal microscope.

2.13 Side population analysis

The fresh tumors were gashed into small squares (approximately 0.5 mm^3) and washed with HBSS containing calcium and magnesium for 3 times. Then, collagenase (100 U/ml, Life Technologies, NY, USA) were added and incubated with tumor tissues for 4 h at 37 °C. Approximately every half an hour, gently agitate the tissue pieces carefully not to let any pieces stick to the side of the tube above the collagenase. The dispersed cells were collected by passing through a sterile nylon mesh and washed with HBSS. Afterward, the cells were stained with Hoechst 33342 dye (5 μg/mL, Invitrogen) in dark for 90 min at 37 °C with shaking every 15 min. At the end of incubation, cells were spun down and re-suspended in ice-cold PBS with 5% FBS. The side population was analyzed with a BD LSR-II Flow Cytometer using a dual wavelength analysis (blue at 450 nm and red at 660 nm) after excitation with 405 nm UV light.

2.14 Biodistribution analysis

For *in vivo* imaging studies, after the tumor reached ~5 mm in diameter, the mice were injected with 100 μl saline, 50 μg ICG in 100 μl saline, and HAC-PFP nanoparticles loaded with ICG (ICG: 50 μg) in 100 μl saline. *In vivo* fluorescence images were taken at 3 and 6 h after intravenous injection via the tail vein using a PerkinElmer (Waltham, MA, USA) IVIS instrument with excitation at 780 nm and an 831 nm filter to collect the fluorescence emission of ICG. After *in vivo* imaging, the mice were sacrificed and the tumor, liver, kidney, lung, spleen, and heart were removed and collected for further *ex vivo* fluorescence imaging of ICG in the organs using the same IVIS instrument.

2.15 Statistical analysis

All data are reported as the mean ± standard deviation (SD) of results from at least three independent runs conducted at three different times. Student's two-tailed *t*-test assuming equal variance was performed to determine the *p* value for assessing statistical significance.

3. Results

3.1. Preparation and characterization of nanoparticles

We prepared the nanoparticles using a modified/improved double-emulsion method. First, PF127, PLGA, and CPT were mixed together in organic solvent (or oil) and emulsified with aqueous solution to form a water-in-oil (W-in-O) structure after the first emulsion where DOX can be encapsulated in the hydrophilic (i.e., aqueous) core dispersed in organic solvent (Fig. 1A). Unlike conventional double-emulsion approach that uses PVA (dissolved in DI water) as the stabilizer during the second emulsion, a mixture of chitosan-PF127 and HA (in deionized or DI water) was used instead in this study (Fig. 1A). During the second emulsion, the hydrophobic portion of chitosan-PF127 should merge into the hydrophobic layer while the hydrophilic part of chitosan-PF127 should stay at the outskirt of the resultant water-in-oil-in-water (W-in-O-in-W) structure of double emulsion. Moreover, the hydrophobic drug

(CPT) dissolved in organic solvent can be encapsulated into the newly formed hydrophobic shell after the second emulsion. DOX can damage DNA via anthracycline-DNA intercalation and inhibit the activity of DNA topoisomerase II [33,34]. CPT is an anti-cancer drug active in the inhibition of DNA topoisomerase I [33,35,36]. Several studies have shown that simultaneous inhibition of topoisomerases II and I could induce a synergistic killing effect on cancer cells [34–36]. Therefore, we hypothesized that our active targeting and dual responsive nanoparticles for co-delivery of DOX and CPT can be used to effectively eliminate the CSCs by inhibiting the four aforementioned mechanisms that contribute to the CSC drug resistance, as illustrated in Fig. 1B.

To confirm successful assembly of PF127 (PF), PLGA (P), chitosan (C)-PF127, and HA within the resultant HAC-PFP nanoparticles, FTIR spectra of all the materials were obtained. As shown in Fig. S1, the spectrum of the HAC-PFP nanoparticles have the characteristic peaks of three (PF127, PLGA, and chitosan-PF127) of the four different starting materials (note: the presence of HA in the HAC-PFP nanoparticles could be judged by the negative surface charge of the nanoparticles to be discussed later), indicating successful preparation of the nanoparticles with the materials using the modified/improved double-emulsion method.

Typical scanning electron microscopy (SEM) images of the HAC-PFP nanoparticles (without drug) together with pure PLGA and PF127 nanoparticles are shown in Fig. 2A. Transmission electron microscopy (TEM) images of HAC-PFP nanoparticles loaded with DOX (D) and CPT (C) (i.e., HAC-PFP-DC nanoparticles) are given in Fig. 2B. Overall, the HAC-PPF nanoparticles either with or without drugs have a uniform size, spherical morphology, and core-shell structure. However, the PLGA nanoparticles prepared in the same way are unstable and tend to form large aggregates (Fig. 2A and Fig. S2), probably due to the hydrophobic nature of the surface of the PLGA nanoparticles. This hypothesis is supported by the milky appearance of the aqueous solution of PLGA nanoparticles (Fig. 2C) as a result of their oil-like surface. In contrast, the solution of HAC-PFP nanoparticles is clear and transparent (so that the colored patterns behind the cuvette could be seen, Fig. 2C), probably due to their hydrophilic surface made of the water soluble polymers (or blocks) including PEG (in PF127), chitosan, and HA. The solution of the HAC-PFP-DC nanoparticles appears clear and reddish. The latter is a result of the red color of DOX. It is worth noting that if only PF127 (or chitosan-PF127) is used to prepare the nanoparticles using the double-emulsion method, few spherical nanoparticles could be obtained (Fig. 2A). Moreover, the PF127 nanoparticles could not be collected by simple centrifugation after synthesis while the HAC-PFP and HAC-PFP-DC nanoparticles could (Fig. 2C with samples in centrifuge tubes). Consequently, the tedious dialysis approach has to be used to clean and collect the PF127 (and most polymeric) nanoparticles. The encapsulated drug will be partially released from the nanoparticles and lost during this lengthy process, which reduces the drug encapsulation efficiency and loading content in the nanoparticles. By combining PF127 and PLGA together, we could overcome all the drawbacks associated with preparing nanoparticles for drug encapsulation using either PF127 or PLGA alone.

Since PF127 is a thermally responsive polymer [27,37], we next investigated if the HAC-PFP nanoparticles possess the thermally responsive property. First, we checked the size of

HAC-PFP nanoparticles made with different ratios of PLGA to PF127 at 22 °C and 37 °C. As shown in Fig. S3, the HAC-PFP nanoparticles are indeed thermally responsive and the ratio of the nanoparticle diameter at 22 °C to that at 37 °C increases slightly with the increase of PF127 in the nanoparticles (the ratios of diameter at 22 °C to that at 37 °C are 1.3, 1.4, and 1.5 for the 1:1, 1:2, and 1:3 ratios of PLGA to PF127, respectively). Moreover, at the 1:2 ratio of PLGA to PF127, the nanoparticles are the smallest and this ratio was used for further studies.

As shown in Fig. 2D, the average diameter of HAC-PFP nanoparticles determined by dynamic light scattering (DLS) is 49.6 ± 2.4 nm at room temperature and it increases to 69.6 ± 7.2 and 91.2 ± 8.1 nm after loading with DOX (i.e., HAC-PFP-D nanoparticles) and both DOX and CPT (i.e., HAC-PFP-DC nanoparticles), respectively. The diameter of HAC-PFP, HAC-PFP-D, and HAC-PFP-DC nanoparticles at 37 °C are 32.8 ± 3.6, 33.1 ± 3.5, and 62.8 ± 1.8 nm, which indicates that the HAC-PFP nanoparticles retain the thermally responsive property after loading with drugs. However, when we adopted the conventionally used 2% PVA instead of HA for stabilizing or preparing the nanoparticles during the second emulsion, the resultant PFP nanoparticles are not thermally responsive and with larger sizes (Fig. S4).

Besides size, the surface zeta potential of the HAC-PFP nanoparticles is also responsive to the change in temperature. As shown in Fig. 2E, when 0.125% HA is used to stabilize the nanoparticles, the zeta potentials of HAC-PFP, HAC-PFP-D, and HAC-PFP-DC nanoparticles are all highly negative at 22 °C (−61.1 ± 0.6, −48.0 ± 1.0, and −60.7 ± 1.0 mV, respectively). When the temperature is increased to 37 °C, the zeta potentials of the HAC-PFP, HAC-PFP-D, HAC-PFP-DC nanoparticles all become highly positive (37.9 ± 0.6, 39.8 ± 1.0, and 26.9 ± 1.3 mV, respectively). These results indicate that more chitosan is exposed on the nanoparticle surface at the higher temperature. If this hypothesis is correct, the surface zeta potential should be lower if more HA is used for preparing/stabilizing the nanoparticles. Indeed, when 0.25% HA is used, the surface zeta potentials of HAC-PFP, HAC-PFP-D and HAC-PFP-DC nanoparticles at 37 °C decrease to −10.3 ± 0.7, −20.2 ± 1.8, and −25.4 ± 1.0 mV, respectively although the zeta potential at 22 °C does not vary much (Fig. 2E).

The aforementioned observations on the nanoparticle size and zeta potential indicate that we have successfully developed thermally responsive nanoparticles using PLGA, PF127 (including chitosan-PF127), and HA. A summary of the size and surface zeta potential determined by DLS at 22 and 37 °C is given in Table S1 for the HAC-PFP, HAC-PFP-D, and HAC-PFP-DC nanoparticles synthesized with 0.25% HA. As the positive surface charge of nanoparticles might interact with blood proteins to reduce the efficiency of *in vivo* drug delivery [38], the nanoparticles synthesized using 0.25% rather than 0.125% HA were used for further studies.

3.2. Characterization of drug encapsulation

In order to confirm both DOX and CPT were encapsulated into the nanoparticles, we checked the fluorescence spectra and UV-Vis absorption of empty and one or two drugs-laden nanoparticles. As shown in Fig. S5, HAC-PFP-D nanoparticles have the spectra of

excitation and emission similar to that of free DOX (with peaks of excitation and emission at 480 and 560–590 nm, respectively). Similarly, the excitation and emission spectra HAC-PFP-C nanoparticles are close to free CPT with peaks of excitation and emission at 370 and 420 nm, respectively (Fig. S6). These data indicate that single drug (hydrophilic DOX or hydrophobic CPT) could be encapsulated into the HAC-PFP nanoparticles with no impact their fluorescence properties. We further confirmed that both drugs were present in the HAC-PFP-DC nanoparticles, probably due to the "green" approach for making the drug-laden nanoparticles. As shown by the fluorescence spectra in Fig. 3A (for excitation) and 3B (for emission), the nanoparticles loaded with two drugs had characteristic excitation and emission peaks of both the hydrophilic DOX and hydrophobic CPT. The UV-Vis absorbance also indicates that the HAC-PFP-D, HAC-PFP-C and HAC-PFP-DC have the specific absorption peaks of DOX (at 486) and/or CPT (at 370 nm) (Fig. 3C).

Interestingly, it was found that the size of HAC-PFP particles was on the micrometer scale before rotary evaporation to remove organic solvent in the double emulsion. As a result, we could take fluorescence image of the particles before removing the organic solvent. As shown in Fig. 3D, both red (DOX) and blue (CPT) fluorescence were detectable in each particle, indicating successful encapsulation of the two drugs within each particle.

At a drug to polymer feeding ratio of 1:20 in weight, the encapsulation efficiency of one drug in the HAC-PFP nanoparticles was 66.6 ± 4.0% for DOX (to form HAC-PFP-D nanoparticles) and 46.6 ± 1.6% for CPT (to form HAC-PFP-C nanoparticles) (Table S2). When co-encapsulating both drugs at the same feeding ratio with the weight ratio of the two drugs being 1:1, the encapsulation efficiency of DOX and CPT was 64.9 ± 4.9% and 38.6 ± 0.4%, respectively. It is worth noting that the conventional double emulsion method is for encapsulating hydrophilic drug only. In our improved double emulsion method, we could also encapsulate hydrophobic drug and importantly, this does not affect the encapsulation efficiency of the hydrophilic drug much.

3.3. pH dependent drug release

For cancer therapy, a nanoparticle system for drug delivery is desired to improve the bioavailability of drugs to tumor while reducing their side effects to normal tissues. This can be achieved by designing nanoparticles with minimal drug release under normal physiological conditions (e.g., pH 7.4) and facilitated drug release in tumor with a low pH (~5–6) [39]. In addition, the uptake of nanoparticles by cancer cells is usually via endocytosis in the late endosome and lysosome with a low pH of ~4–5 [40]. Therefore, we investigated the *in vitro* drug release at 37 °C from the HA (HAC-PFP-DC) versus PVA (PFP-DC) stabilized nanoparticles at both pH 7.4 and 5.0 (Fig. 3E). At pH 7.4, the release of CPT and DOX was slow/sustained from both the HAC-PFP-DC and PFP-DC nanoparticles: ~64% of CPT and ~30% of DOX was released within 72 h. The release of both drugs from the HAC-PFP-DC and PFP-DC nanoparticles was faster at pH 5.0. Moreover, the HAC-PFP-DC nanoparticles are much more responsive to low pH than the PFP-DC nanoparticles: 50% percent of CPT was released from HAC-PFP-DC nanoparticles in only 4.4 h while it took 23.2 h to release the same amount of CPT from the PFP-DC nanoparticles at pH 5.0. For

DOX, 50% of the drug was released at pH 5.0 from the HAC-PFP-DC and PFP-DC nanoparticles in 6.1 and 42.4 h, respectively.

We used HA to stabilize the nanoparticles by utilizing the electrostatic interactions between HA (negatively charged) and chitosan (positively charged) at pH 7.4. In an acidic solution, the equilibrium of this interaction at pH 7.4 is broken and the two polymers dissociate. As a result, the HAC-PFP-DC nanoparticles are unstable in acidic solutions. As an uncharged polymer, PVA would not be affected much by the pH change and the PFP-DC nanoparticles are more stable at and less responsive to low pH than the HAC-PFP-DC nanoparticles. To confirm this hypothesis, studies were conducted to examine the stability of the HAC-PFP-DC versus PFP-DC nanoparticles at low pH by dissolving the nanoparticles in acidic solution (pH 5.0) and incubating at 37 °C for 3 h. As shown in Fig. 3F, the PFP-DC nanoparticles still have an intact core-shell structure in the acidic solution. By contrast, the core-shell structure of HAC-PFP-DC nanoparticles was compromised (arrows). Some of the HAC-PFP-DC nanoparticles even disassembled in the acidic solution with the formation of smaller sized nanoparticles according to the TEM image. We further checked the size of PFP and HAC-PFP nanoparticles at pH 7.4 and 5.0 using DLS. As shown in Fig. 3G, the average size of PFP nanoparticles did not changed much between pH 7.4 and 5.0. However, the average size of HAC-PFP-DC reduced from 91.2 ± 8.1 at pH 7.4 to 46.9 ± 2.7 nm at pH 5.0.

3.4. Cellular uptake and intracellular distribution in 3D spheroids enriched with CSCs

To examine the capability of targeted delivery using our HA-decorated nanoparticles to MDA-MB-231 mammary and PC-3 prostate CSCs, we incubated MDA-MB-231 mammospheres and PC-3 prostaspheres (both were enriched with CSCs) with the mixture of the two free drugs (DOX&CPT with DOX:CPT = 1:1), PFP-DC, and HAC-PFP-DC for 3 h. As shown in Fig. 4A (for PC-3 prostaspheres) and 4B (for MDA-MB-231 mammospheres), free DOX could enter the mammosphere and prostasphere cells (enriched with CSCs) as a result of its hydrophilic or water-soluble nature, probably by passive diffusion. However, there was almost no free CPT in the mammosphere and prostasphere cells, probably due to its hydrophobic or water-insoluble nature with low bioavailability to the cells. After being encapsulated into PFP-DC nanoparticles, both drugs could be taken up by the 3D cultured cells after 3 h incubation. Moreover, the uptake could be further improved (particularly for CPT) with the use of HAC-PFP-DC nanoparticles, suggesting active targeting via the interaction of HA on the nanoparticle surface and CD44 overexpressed on the mammosphere and prostasphere cells. It is worth noting that there is significant overlap between the two drugs delivered by the two nanoparticles and the green stain of late endosomes/lysosomes while such overlap is minimal for free DOX, according to Fig. 4A–B. Moreover, the overlap is more extensive between late endosomes/lysosomes and DOX than CPT, which might be due to the much faster release of CPT than DOX from the nanoparticles in acidic endosomes/lysosomes (Fig. 3E). These observations confirm that the cells actively took up the encapsulated drug via endocytosis while the free DOX entered the cells by passive diffusion.

We further quantified cellular uptake of the various drug formulations using flow cytometry. As shown in Fig. 4C, the DOX and CPT fluorescence intensity in both the mammosphere

and prostasphere cells is consistent with the confocal microscopy data shown in Fig. 4A–B. Only the HAC-PFP-DC nanoparticles could efficiently deliver both drugs into both the mammosphere and prostasphere cells. According to the *in vitro* drug release profiles, HAC-PFP-DC could also release the drug quickly in the acidic late endosomes/lysosomes, which may help to enhance the cytotoxicity of DOX and CPT to destroy the mammosphere and prostasphere cells enriched with CSCs.

3.5. Destruction of 3D prostaspheres and mammospheres enriched with CSCs in vitro

To investigate the potentially enhanced anticancer capacity of HAC-PFP-DC nanoparticles, PC-3 prostaspheres and MDA-MB-231 mammospheres enriched with CSCs were treated with free DOX, simple mixture of free DOX&CPT, HAC-PFP-D, PFP-DC, and HAC-PFP-DC at various concentrations (DOX:CPT = 1:1 for all two-drug formulations). The viability data are shown in Fig. 5A. According to the figure, the HAC-PFP nanoparticles without any drug were not harmful to the cells, suggesting the superior biocompatibility of the nanoparticles. This is probably due to the fact that they are made of biocompatible polymers that are already approved by the FDA for medical use. Interestingly, both the PFP-DC (without HA decoration on the surface) and HAC-PFP-D (encapsulated with DOX only) appear to be even less cytotoxic than free DOX. This is probably due to the delayed release of DOX from the nanoparticles (Fig. 3E), which reduces the bioavailability of the water-soluble drug to the cells during the incubation period. More importantly, the HAC-PFP-DC nanoparticles exhibit the highest cytotoxicity compared to all the other formulations. This is probably due to multiple mechanisms including the capability of DOX and CPT in killing the prostasphere and mammosphere cells by inhibiting the activities of both topoisomerase I and II, active targeting the cells by HA, small size (10–100 nm) (at 37 °C due to thermal responsiveness) that facilitates cell uptake of the nanoparticles by endocytosis [28,41], and pH responsiveness to induce quick release of drugs in late endosome/lysosome with a low pH.

We further quantified the IC50 (inhibitory concentration to kill 50% cells) with SPSS (Chicago, IL, USA) by interpolation using the cell viability data shown in Fig. 5A. As shown in Fig. 5B, the IC50 of HAC-PFP-DC nanoparticles is 82.2 ± 13.9 nM for PC-3 prostasphere cells, which is ~6.7, 2.8, 15.8, and 66.3 times lower than that of free DOX, DOX&CPT, HAC-PFP-D nanoparticles, and PFP-DC nanoparticles, respectively. For MDA-MB-231 mammosphere cells, the IC50 for HAC-PFP-DC nanoparticles is 42.1 ± 3.5 nM, which is ~41.7, 205.0, 381.9, and 419.1 times lower than free DOX, DOX&CPT, HAC-PFP-D nanoparticles, and PFP-DC nanoparticles, respectively. Considering that the CSCs are usually less than ~15% of the overall cell population in the prostaspheres and mammospheres [31,32,42], we further quantified the IC85 (inhibitory concentration to kill 85% cells) with SPSS for the various drug formulations to ensure the effect of CSCs is accounted for the comparison. As shown in Fig. 5C, the IC85 of HAC-PFP-DC nanoparticles is 1.3 ± 0.1 μM for the PC-3 prostasphere cells, which is ~16, 19, 125, and 511 times lower than that of free DOX, DOX&CPT, HAC-PFP-D nanoparticles, and PFP-DC nanoparticles, respectively. The IC85 of HAC-PFP-DC nanoparticles for MDA-MB-231 mammosphere cells is 78.2 ± 55.2 μM, which is ~9, 8, 14, and 27 times lower than that of free DOX, DOX&CPT, HAC-PFP-D nanoparticles, and PFP-D nanoparticles, respectively.

Besides cell viability, we further quantified the change in area of the 3D prostaspheres and mammospheres treated with the four different drug (1.7 μM) formulations together with no treatment (NT) over 10 days. The quantitative and qualitative data are shown in Fig. 5D and 5E, respectively. With no treatment, the area of both the PC-3 prostaspheres and MDA-MB-231 mammospheres doubled after 10-day culture. The treatments with free DOX, DOX&CPT, and PFP-DC nanoparticles could significantly inhibit the *in vitro* tumor growth, but only reduced the tumors to ~60–70% of their initial area. Remarkably, the HAC-PFP-DC nanoparticles could reduce the area to ~3% and 20% of the initial area for the PC-3 prostaspheres and MDA-MB-231 mammospheres, respectively.

All the aforementioned data indicate that the prostasphere and mammosphere cells enriched with CSCs are highly resistant to the free anticancer drugs, which could be effectively and significantly reduced by using HAC-PFP-DC nanoparticles. Therefore, we are curious about the possible mechanisms of the nanoparticles in destroying the prostasphere and mammosphere cells enriched with the CSCs *in vitro*, for which we first investigated the expression of CD44 and CD133 on the mammosphere and prostasphere cells that survived the free DOX treatment for 10 days using flow cytometry. As shown in Fig. S7A, the cells that survived free DOX treatment expressed more CD44 than the prostasphere/mammosphere cells before treatment although the expression of CD133 did not change much. Since CD44 is a commonly used marker of CSCs, these results indicate that the CSCs are highly resistant to the free drug treatment. However, for HAC-PFP-DC nanoparticles, the more CD44 expression on cell membrane, the more nanoparticles could bind to the receptor. As a result, more DOX and CPT could be delivered into the CSCs using the HAC-PFP-DC nanoparticles to effectively destroy the *in vitro* tumor with minimal cell survival as shown in Fig. 5E.

DOX has been shown to be a cell-cycle nonspecific anticancer drug [43] while CPT is a cell-cycle specific drug that mainly causes S-phase-specific cell killing [44]. Therefore, we next investigated the cell-cycle distribution of the PC-3 prostasphere cells either with no treatment (NT) or treated by free DOX, free CPT, or HAC-PFP-DC nanoparticles for 48 h using flow cytometry. As shown in Fig. S7B, the free DOX treatment reduced the peak of the G_2/M phase with an increase of cells in the G_1/G_0 phase whereas the free CPT treatment significantly increased cells in the G_1/G_0 phase with a reduction of cells in both the S and G_2/M phases, compared to the cells with no treatment. For the HAC-PFP-DC treated group, many of the cells were apoptotic and there were no cells in the S phase.

3.6. Enhanced antitumor efficacy in vivo of HAC-PFP-DC nanoparticles

Lastly, we treated orthotopic MDA-MB-231 (triple-negative) human mammary tumor-bearing mice with different drug formulations to understand the safety and efficacy of the HAC-PFP-DC nanoparticles for cancer therapy. The tumors was produced by injecting 20,000 MDA-MB-231 mammosphere cells per mouse into the fat pad of 6–8 week-old female nude mice. The tumor-bearing mice were randomly divided into 6 groups: saline, blank nanoparticles (HAC-PFP), free DOX&CPT, HAC-PFP-D nanoparticles, PFP-DC nanoparticles, and HAC-PFP-DC nanoparticles. Mice were treated with the various drug formations at a total dose of 3 mg/kg (for two-drug formations: DOX: 1.5 mg/kg and CPT:

1.5 mg/kg) body weight via intravenous injection when the tumor reached a volume of ~100 mm^3 for a total of times (on days 1, 7, and 14). No mice died during the course of the one-month treatment and observation. As shown in Fig. 6A–B, tumor growth for treatments with blank HAC-PFP nanoparticles is similar to that of saline control. The change in tumor volume for the treatment with free DOX&CPT is also not significantly different from that of the saline control. For the treatment with HAC-PFP-D and PFP-DC nanoparticles, tumor volume was significantly decreased compared to the saline control. Importantly, the HAC-PFP-DC nanoparticles exhibit the best anti-tumor capacity and gradually reduced the tumor volume during the entire observation period. The size and weight of the tumors in the HAC-PFP-DC treated group are significantly less than that from the other treatment groups (Fig. 6C). Moreover, histological examination (H&E stain) revealed extensive necrosis in the tumors from the HAC-PFP-DC group while tumors from the other groups were more viable (Fig. 6D). Extensive early (Annexin V staining) and late (propidium iodide or PI staining) apoptosis is observable for tumors from the HAC-PFP-DC group while minimal apoptosis shows up in the other groups (Fig. 6E). Collectively, these data demonstrate the remarkable *in vivo* anti-tumor efficacy of the HAC-PFP-DC nanoparticles.

Equally important, we did not notice any obvious sign of side effects for the HAC-PFP-DC nanoparticles. Neither death nor significant drop of body weight was noted for the mice treated with saline, blank HAC-PFP nanoparticles, and all the four drug formulations (Fig. 6F). Major organs from the HAC-PFP-DC treated mice were collected at 30 days after the treatment for histology analysis. No obvious damage to the critical organs was observable in the H&E stained tissue slices (Fig. S8). These results indicate the superior safety of the HAC-PFP nanoparticles for delivering therapeutic agents *in vivo*.

3.7. In vivo biodistribution of HAC-PFP nanoparticles and analysis of CSCs in tumors post treatment

To understand the enhanced *in vivo* anti-tumor capacity of the two drugs-laden HAC-PFP nanoparticles by evaluating their biodistribution *in vivo*, indocyanine green (ICG) that has been clinically used for noninvasive imaging was encapsulated into the HAC-PFP nanoparticles in the same way as that for encapsulating DOX. As shown in Figs. 7A and S9, highly enhanced fluorescence of ICG was observable in tumor at 3 h and 6 h after intravenous injection of the HAC-PFP nanoparticle-encapsulated ICG, compared to free ICG. To confirm the observation from whole animal imaging, various organs were harvested for *ex vivo* imaging to check the distribution of ICG after sacrificing the mice at 6 h. Only tumors from the HAC-PFP group show strong fluorescence of ICG (Fig. 7B). These observations indicate the excellent capability of HAC-PFP nanoparticles in targeting tumor *in vivo*, which may explain the superb anti-tumor capacity of the HAC-PFP-DC shown in Fig. 6.

We further analyzed the CSC subpopulations in the *in vivo* tumors after treated with various drug formulations using flow cytometry. The subpopulation of cancer cells (often called the side population) capable of excluding Hoechst 33342 has been taken as one of the rare CSC subpopulations. Typical images of two-channel flow cytometry showing distinct side populations (in the boxed region) and the percentage data from three independent runs are

given in Fig. 7C and 7D, respectively. A significantly lower percentage of the side population was consistently observed in the HAC-PFP-DC treated tumors on day 30, which further support the capability of the HAC-PFP-DC nanoparticles in targeting and destroying the CSCs.

CD44 is a multi-structural and multi-functional cell surface receptor involved in cell proliferation, cell differentiation, cell migration, and angiogenesis [45], while CD133 is believed to be associated with tumorigenicity and progression of the disease [46]. Both CD44 and CD133 have been commonly used as the surface markers of CSCs [31,32,42]. Therefore, we checked the expression of CD44 and CD133 on cancer cells in the *in vivo* tumors after the various treatments. Typical micrographs of immunohistochemical staining showing high expression of the two markers in tumors treated with saline, HAC-PFP nanoparticles, DPX&CPT, and HAC-PFP-D nanoparticles (Figs. 7E and S10 for high and low magnifications, respectively). Interestingly, reduced expression of CD44 and CD133 is evident in tumors treated with both PFP-DC and HAC-PFP-DC nanoparticles, which suggests that the combination of DOX and CPT is effective for destroying the $CD44^{+}CD133^{+}$ CSCs. Furthermore, the expression of CD44 and CD133 in tumors treated with the HAC-PFP-DC nanoparticles is negligible, indicating the importance of actively targeting CSCs with HA for effective destruction of the CSCs.

4. Discussion

Unlike the conventional double-emulsion approach for which PVA (dissolved in DI water) was used as the stabilizer during the second emulsion, a mixture of chitosan-PF127 and HA (dissolved in DI water) were used instead in this study (Fig. 1). Conventionally, a total of 2% PVA (dissolved in DI water) has been used to stabilize the nanoparticles. In this study, we found that probably due to the electrostatic interaction between HA (negative) and chitosan (positive), only 0.125% HA (dissolved in DI water) is sufficient to effectively stabilize the nanoparticles. Moreover, because of the specific binding between HA (a natural ligand of CD44 in the extracellular matrix of tumor) and CD44, our nanoparticles can be used for targeted delivery of anticancer drugs into CSCs that are commonly overexpressed with CD44.

Furthermore, unlike PVA that is probably entangled on the entire surface of nanoparticles, HA is probably adsorbed only on the nanoparticle surface where chitosan locates through electrostatic interactions without much entanglement. In other words, HA could rearrange on the nanoparticle surface together with chitosan to allow the nanoparticles to easily change in size and surface zeta potential in response to the change in temperature (Fig. 2D–E). This may explain why the HA stabilized nanoparticles are thermally responsive while the PVA stabilized nanoparticles are not. This may also explain the much faster release of DOX and CPT from the HAC-PFP-DC than the PFP-DC nanoparticles at pH 5.0 (Fig. 3E). This acidic pH can break the equilibrium of electrostatic interaction between HA and chitosan established at neutral pH during synthesis, leading to the dissociation of HA and chitosan in the HAC-PFP-DC nanoparticles (but not the PFP-DC nanoparticles) and further detachment and disassembly of the nanoparticles ensues (Fig. 3F). A schematic illustration and summary of the aforementioned probable mechanisms of drug release at both pH 7.4 and 5.0 for the

two different types of nanoparticles is given in Fig. S11. In brief, the HAC-PFP-DC nanoparticles demonstrate enhanced pH-responsiveness for quick drug release in acidic environments compared to PFP-DC nanoparticles although both types of nanoparticles can be used to achieve sustained release at neutral pH. In addition, this simple electrostatic interaction rather than covalent bonding between HA and chitosan may help to retain the capability of HA in targeting the CSCs as demonstrated by the data shown in Figs. 4–7 (for HAC-PFP-DC versus PFP-DC nanoparticles).

It is worth noting that we did not observe a burst release of either drug from either the HAC-PFP-DC or PFP-DC nanoparticles when heating the samples from 22 to 37 °C for the drug release studies (Fig. 3E). This is not surprising for the PFP-DC nanoparticles since they are not thermally responsive (Fig. S4). The negligible release of either drug from the thermally responsive HAC-PFP-DC nanoparticles suggests that the reduction of size of the nanoparticles from 22 to 37 °C is mainly a result of shrinking in the outermost hydrophilic wall/shell and in the hydrophobic shell in the nanoparticles with minimal change in the size of their hydrophilic core (so that release of the DOX from the hydrophilic core is negligible during heating).

DOX can damage DNA via inhibition of topoisomerase II (in addition to anthracycline-DNA intercalation) while the anticancer activity of CPT is a result of its capability of inhibiting DNA topoisomerase I [33]. Both topoisomerases II and I are essential enzymes during DNA replication and gene transcription. Topoisomerase I can generate single-stranded DNA breaks by cutting DNA strand and allowing rotation of the cleaved strand to alter the pitch of DNA double helices [47]. Topoisomerase II regulates the DNA topology by transient cleavage, strand passing, and re-ligation of double-stranded DNA [47]. Both topoisomerases II and I are indispensible for DNA replication during the S phase of cell cycle. This may explain why there were no cells left in the S phase after treatment with HAC-PFP-DC (Fig. S7B), which further resulted in more apoptosis of cells treated with the HAC-PFP-DC nanoparticles *in vitro* (Fig. S7B) and *in vivo* (Fig. 6E). In other words, the HAC-PFP-DC nanoparticles can be used to fight against the enhanced capability of anti-apoptosis of cancer cells and particularly the CSCs. These observations are consistent with previous reports showing that simultaneous inhibition of topoisomerases II and I could induce a synergistic effect against cancer [34–36]. The high drug resistance of CSCs has been partially attributed to their enhanced capability of DNA repair and anti-apoptosis. Besides DNA replication, topoisomerases I and II are important for transcription, DNA recombination, DNA reparation, chromosome condensation, and sister chromatid segregation [48]. Therefore, the synergistic effects of this two-drug combination may exist in term of not only cell cycle but also the combat against the drug resistant mechanisms of CSCs.

5. Conclusion

In summary, we have developed novel HAC-PFP-DC nanoparticles composed of HA, PLGA, chitosan (minimal), and PF127 with both thermal and pH responsiveness for targeted co-delivery of both hydrophilic (DOX) and hydrophobic (CPT) chemotherapeutics into human mammary and prostate CSCs. With PF127, we have prepared more stable and uniform PLGA-based nanoparticles with thermal responsiveness and excellent aqueous

solubility. An ~10 times lower concentration of HA, instead of PVA, could be used as the stabilizer for preparing the nanoparticles with the double-emulsion method, which allows for active targeting of the CSCs and acidic pH-triggered drug release. The HAC-PFP-DC nanoparticles demonstrate high efficacy against both the prostasphere and mammosphere cells enriched with CSCs *in vitro* and CSCs in human breast tumor *in vivo*. This is probably due to the synergistic anticancer activities of DOX and CPT and the capability of the nanoparticles in actively targeting CSCs, delivering more drugs into the CSCs as a result of their dual responsiveness, and releasing the drug quickly inside the cytosol away from the plasma membrane to overcome the four possible mechanisms of high drug resistance by CSCs as summarized and illustrated in Fig. 1. Our extensive *in vitro* studies with the 3D microscale tumors (i.e., prostaspheres and mammospheres) enriched with CSCs and *in vivo* studies using orthotopic human breast tumors grown in mice demonstrate the potential of the co-delivery of DOX and CPT in one nanoparticle capable of active targeting and dual responsiveness in overcoming the drug resistance of the CSCs-the root of cancer metastasis and recurrence.

Supplementary Material

Refer to Web version on PubMed Central for supplementary material.

Acknowledgments

This work was supported by an American Cancer Society (ACS) Research Scholar Grant (# 120936-RSG-11-109-01-CDD) to XH and a Pelotonia postdoctoral fellowship to HW. We thank Jenna Dumbleton for proofreading the manuscript.

Appendix A. Supplementary Data

Supplementary data related to this article can be found at http://

References

1. Jordan CT, Guzman ML, Noble M. Cancer stem cells. N Engl J Med. 2006; 355:1253–61. [PubMed: 16990388]
2. Liu C, Kelnar K, Liu B, Chen X, Calhoun-Davis T, Li H, et al. The microRNA miR-34a inhibits prostate cancer stem cells and metastasis by directly repressing CD44. Nat Med. 2011; 17:211–5. [PubMed: 21240262]
3. Gilbert CA, Ross AH. Cancer stem cells: cell culture, markers, and targets for new therapies. J Cell Biochem. 2009; 108:1031–8. [PubMed: 19760641]
4. Chin AR, Wang SE. Cytokines driving breast cancer stemness. Mol Cell Endocrinol. 2014; 382:598–602. [PubMed: 23562748]
5. Korkaya H, Liu S, Wicha MS. Breast cancer stem cells, cytokine networks, and the tumor microenvironment. J Clin Invest. 2011; 121:3804–9. [PubMed: 21965337]
6. Visvader JE, Lindeman GJ. Cancer stem cells in solid tumours: accumulating evidence and unresolved questions. Nat Rev Cancer. 2008; 8:755–68. [PubMed: 18784658]
7. Singh A, Settleman J. EMT, cancer stem cells and drug resistance: an emerging axis of evil in the war on cancer. Oncogene. 2010; 29:4741–51. [PubMed: 20531305]
8. Zeng X, Morgenstern R, Nystrom AM. Nanoparticle-directed sub-cellular localization of doxorubicin and the sensitization breast cancer cells by circumventing GST-mediated drug resistance. Biomaterials. 2014; 35:1227–39. [PubMed: 24210875]

9. Hu CM, Zhang L. Nanoparticle-based combination therapy toward overcoming drug resistance in cancer. Biochemical pharmacology. 2012; 83:1104–11. [PubMed: 22285912]
10. Peer D, Karp JM, Hong S, Farokhzad OC, Margalit R, Langer R. Nanocarriers as an emerging platform for cancer therapy. Nat Nanotechnol. 2007; 2:751–60. [PubMed: 18654426]
11. El-Dakdouki MH, Xia J, Zhu DC, Kavunja H, Grieshaber J, O'Reilly S, et al. Assessing the in vivo efficacy of doxorubicin loaded hyaluronan nanoparticles. ACS applied materials & interfaces. 2014; 6:697–705. [PubMed: 24308364]
12. Mo R, Jiang T, DiSanto R, Tai W, Gu Z. ATP-triggered anticancer drug delivery. Nature communications. 2014; 5:3364.
13. Ruiz-Esparza GU, Wu S, Segura-Ibarra V, Cara FE, Evans KW, Milosevic M, et al. Polymer Nanoparticles Encased in a Cyclodextrin Complex Shell for Potential Site-and Sequence-Specific Drug Release. Adv Funct Mater. 2014; 24:4753–61.
14. Cheng R, Meng FH, Deng C, Klok HA, Zhong ZY. Dual and multi-stimuli responsive polymeric nanoparticles for programmed site-specific drug delivery. Biomaterials. 2013; 34:3647–57. [PubMed: 23415642]
15. Bertrand N, Wu J, Xu XY, Kamaly N, Farokhzad OC. Cancer nanotechnology: The impact of passive and active targeting in the era of modern cancer biology. Adv Drug Deliv Rev. 2014; 66:2–25. [PubMed: 24270007]
16. Koval M, Preiter K, Adles C, Stahl PD, Steinberg TH. Size of IgG-opsonized particles determines macrophage response during internalization. Exp Cell Res. 1998; 242:265–73. [PubMed: 9665824]
17. Sahoo SK, Labhasetwar V. Enhanced antiproliferative activity of transferrin-conjugated paclitaxel-loaded nanoparticles is mediated via sustained intracellular drug retention. Mol Pharm. 2005; 2:373–83. [PubMed: 16196490]
18. Albanese A, Walkey CD, Olsen JB, Guo H, Emili A, Chan WC. Secreted biomolecules alter the biological identity and cellular interactions of nanoparticles. ACS Nano. 2014; 8:5515–26. [PubMed: 24797313]
19. Holohan C, Van Schaeybroeck S, Longley DB, Johnston PG. Cancer drug resistance: an evolving paradigm. Nature reviews Cancer. 2013; 13:714–26. [PubMed: 24060863]
20. Pommier Y. Topoisomerase I inhibitors: camptothecins and beyond. Nat Rev Cancer. 2006; 6:789–802. [PubMed: 16990856]
21. Hirose S, Suzuki Y. In vitro transcription of eukaryotic genes is affected differently by the degree of DNA supercoiling. Proc Natl Acad Sci. 1988; 85:718–22. [PubMed: 2829200]
22. Liu LF, Wang JC. Supercoiling of the DNA template during transcription. Proc Natl Acad Sci. 1987; 84:7024–7. [PubMed: 2823250]
23. Hu CM, Aryal S, Zhang L. Nanoparticle-assisted combination therapies for effective cancer treatment. Therapeutic delivery. 2010; 1:323–34. [PubMed: 22816135]
24. Auzenne E, Ghosh SC, Khodadadian M, Rivera B, Farquhar D, Price RE, et al. Hyaluronic acid-paclitaxel: antitumor efficacy against CD44 (+) human ovarian carcinoma xenografts. Neoplasia. 2007; 9:479–86. [PubMed: 17603630]
25. Jordan CT, Guzman ML, Noble M. Cancer stem cells. New England Journal of Medicine. 2006; 355:1253–61. [PubMed: 16990388]
26. Vinogradov S, Wei X. Cancer stem cells and drug resistance: the potential of nanomedicine. Nanomedicine. 2012; 7:597–615. [PubMed: 22471722]
27. Zhang W, Gilstrap K, Wu L, K CR, Moss MA, Wang Q, et al. Synthesis and characterization of thermally responsive Pluronic F127-chitosan nanocapsules for controlled release and intracellular delivery of small molecules. ACS nano. 2010; 4:6747–59. [PubMed: 21038924]
28. Rao W, Zhang W, Poventud-Fuentes I, Wang Y, Lei Y, Agarwal P, et al. Thermally responsive nanoparticle-encapsulated curcumin and its combination with mild hyperthermia for enhanced cancer cell destruction. Acta Biomater. 2014; 10:831–42. [PubMed: 24516867]
29. Zhang W, Rong J, Wang Q, He X. The encapsulation and intracellular delivery of trehalose using a thermally responsive nanocapsule. Nanotechnology. 2009; 20:275101. [PubMed: 19528681]

30. Wang H, Zhao Y, Wu Y, Hu YL, Nan K, Nie G, et al. Enhanced anti-tumor efficacy by co-delivery of doxorubicin and paclitaxel with amphiphilic methoxy PEG-PLGA copolymer nanoparticles. Biomaterials. 2011; 32:8281–90. [PubMed: 21807411]
31. Rao W, Bellotti A, Littrup PJ, Yu J, Lu X, He X. Nanoparticle-encapsulated doxorubicin enhances cryoablation of cancer stem-like cells. Technology. 2014; 2:28–35.
32. Rao W, Zhao S, Yu J, Lu X, Zynger DL, He X. Enhanced enrichment of prostate cancer stem-like cells with miniaturized 3D culture in liquid core-hydrogel shell microcapsules. Biomaterials. 2014; 35:7762–73. [PubMed: 24952981]
33. Pommier Y, Leo E, Zhang H, Marchand C. DNA topoisomerases and their poisoning by anticancer and antibacterial drugs. Chemistry & biology. 2010; 17:421–33. [PubMed: 20534341]
34. Nishimura S, Tsuda H, Hashiguchi Y, Kokawa K, Nishimura R, Ishiko O, et al. Phase II study of irinotecan plus doxorubicin for early recurrent or platinum-refractory ovarian cancer: interim analysis. International journal of gynecological cancer: official journal of the International Gynecological Cancer Society. 2007; 17:159–63. [PubMed: 17291248]
35. Cortes F, Pinero J. Synergistic effect of inhibitors of topoisomerase I and II on chromosome damage and cell killing in cultured Chinese hamster ovary cells. Cancer chemotherapy and pharmacology. 1994; 34:411–5. [PubMed: 8070008]
36. Kim R, Hirabayashi N, Nishiyama M, Jinushi K, Toge T, Okada K. Experimental studies on biochemical modulation targeting topoisomerase I and II in human tumor xenografts in nude mice. Int J Cancer. 1992; 50:760–6. [PubMed: 1312063]
37. Jen MC, Serrano MC, van Lith R, Ameer GA. Polymer-Based Nitric Oxide Therapies: Recent Insights for Biomedical Applications. Adv Funct Mater. 2012; 22:239–60. [PubMed: 25067935]
38. Sun T, Zhang YS, Pang B, Hyun DC, Yang M, Xia Y. Engineered Nanoparticles for Drug Delivery in Cancer Therapy. Angew Chem Int Ed Engl. 2014; 53:12320–64. [PubMed: 25294565]
39. Wang H, Zhao Y, Wu Y, Hu Y-L, Nan K, Nie G, et al. Enhanced anti-tumor efficacy by co-delivery of doxorubicin and paclitaxel with amphiphilic methoxy PEG-PLGA copolymer nanoparticles. Biomaterials. 2011; 32:8281–90. [PubMed: 21807411]
40. Su S, Wang H, Liu X, Wu Y, Nie G. iRGD-coupled responsive fluorescent nanogel for targeted drug delivery. Biomaterials. 2013; 34:3523–33. [PubMed: 23410678]
41. Gao H, Shi W, Freund LB. Mechanics of receptor-mediated endocytosis. Proc Natl Acad Sci U S A. 2005; 102:9469–74. [PubMed: 15972807]
42. Rao W, Wang H, Han J, Zhao S, Dumbleton J, Agarwal P, et al. Chitosan-Decorated Doxorubicin-Encapsulated Nanoparticle Targets and Eliminates Tumor Reinitiating Cancer Stem-Like Cells. ACS Nano. 2015; 9:5725–40. [PubMed: 26004286]
43. Gardner SN. A mechanistic, predictive model of dose-response curves for cell cycle phase-specific and -nonspecific drugs. Cancer research. 2000; 60:1417–25. [PubMed: 10728708]
44. Xu Y, Villalona-Calero MA. Irinotecan: mechanisms of tumor resistance and novel strategies for modulating its activity. Annals of oncology: official journal of the European Society for Medical Oncology / ESMO. 2002; 13:1841–51. [PubMed: 12453851]
45. Marhaba R, Zöller M. CD44 in cancer progression: adhesion, migration and growth regulation. Journal of molecular histology. 2004; 35:211–31. [PubMed: 15339042]
46. Sahlberg SH, Spiegelberg D, Glimelius B, Stenerlöw B, Nestor M. Evaluation of cancer stem cell markers CD133, CD44, CD24: association with AKT isoforms and radiation resistance in colon cancer cells. PloS one. 2014; 9:e94621. [PubMed: 24760019]
47. Meyer KN, Kjeldsen E, Straub T, Knudsen BR, Hickson ID, Kikuchi A, et al. Cell cycle-coupled relocation of types I and II topoisomerases and modulation of catalytic enzyme activities. J Cell Biol. 1997; 136:775–88. [PubMed: 9049244]
48. Wang JC, Caron PR, Kim RA. The role of DNA topoisomerases in recombination and genome stability: a double-edged sword? Cell. 1990; 62:403–6. [PubMed: 2165864]

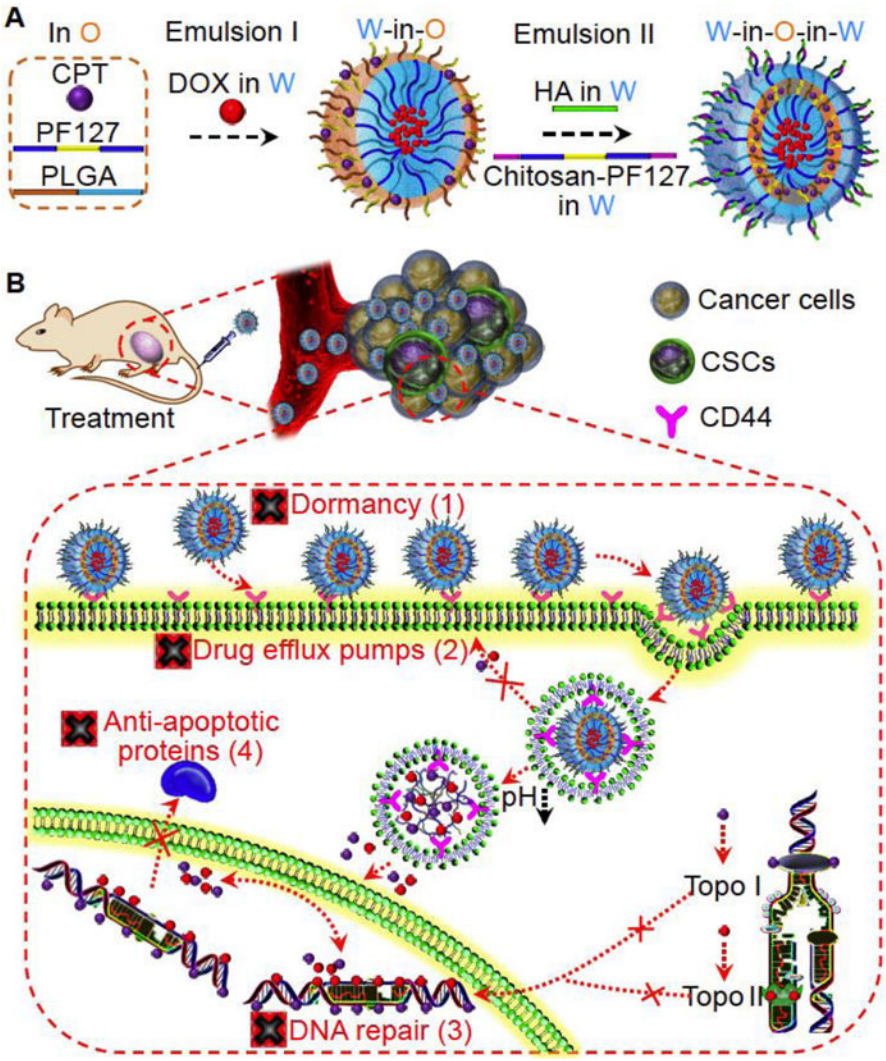

Fig. 1.

A schematic illustration of the procedure for preparing nanoparticles and their capability of targeting four different drug resistant mechanisms of cancer stem-like cells (CSCs). (A) Hyaluronic acid (HA), PF127 (PF, with and without chitosan modification), and PLGA (P) were used to prepare the DOX (D) and CPT (C)-laden HAC-PFP-DC nanoparticles using an improved double-emulsion method. (B) The HAC-PFP-DC nanoparticles can be used to fight against the multifaceted mechanisms of drug resistance of CSCs including their capability of actively targeting CSCs to facilitate drug uptake by the cells to reduce their drug resistance due to dormancy or slow metabolic activity (1); delivery and release of drugs away from the plasma membrane to minimize the drug efflux by the transmembrane pumps of CSCs (2); and co-delivery of two chemotherapeutic drugs (DOX and CPT) that synergistically inhibit the activity of topoisomerases I and II that are crucial for DNA repair and production of anti-apoptotic proteins to combat against the drug resistance of CSCs due to their enhanced capability of DNA repair (3) and anti-apoptosis (4). O: oil (i.e., organic solvent), W: water, DOX: doxorubicin hydrochloride, CPT: irinotecan, PLGA: poly (D,L-lactide-co-glycolide), and Topo: topoisomerase.

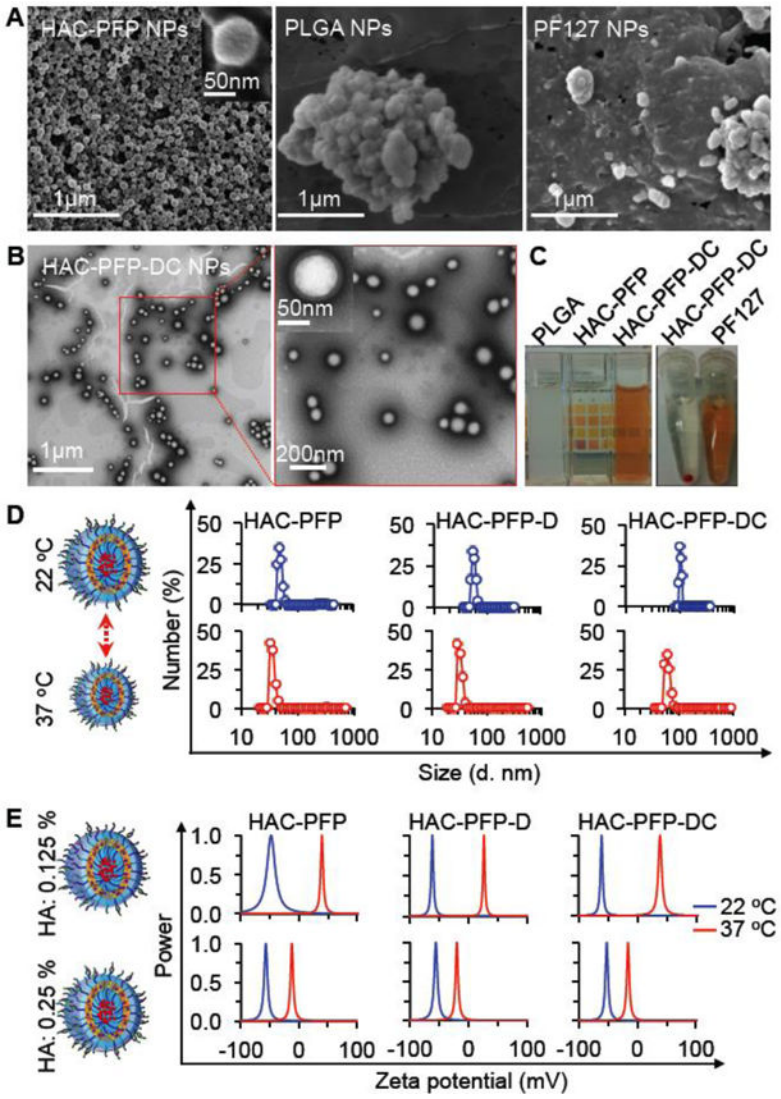

Fig. 2.

Nanoparticle characterization showing the uniform size, core-shell morphology, high aqueous solubility, and thermal responsiveness of the HAC-PFP nanoparticles. (A) SEM images of HAC-PFP, PLGA, and PF127 nanoparticles. (B) TEM images of HAC-PFP nanoparticles after loading with DOX and CPT (i.e., HAC-PFP-DC nanoparticles) at two different magnifications. (C) A typical picture of PLGA, HAC-PFP, HAC-PFP-DC, and PF127 nanoparticles in water where the two samples in the 1.5 ml centrifuge tubes are after centrifugation. (D) Size distribution of HAC-PFP, HAC-PFP-D, and HAC-PFP-DC nanoparticles determined by dynamic light scattering (DLS) at 22 and 37 °C. (E) Surface zeta potential of HAC-PFP, HAC-PFP-D, and HAC-PFP-DC nanoparticles synthesized with different percentages of HA at 22 °C and 37 °C. Collectively, the data show the round and core-shell morphology of the HAC-PFP nanoparticles (with or without drugs) together with their several advantages to the nanoparticles made of PLGA or PF127 alone including uniform size, convenient collection by centrifugation, and thermal responsiveness in size and surface change.

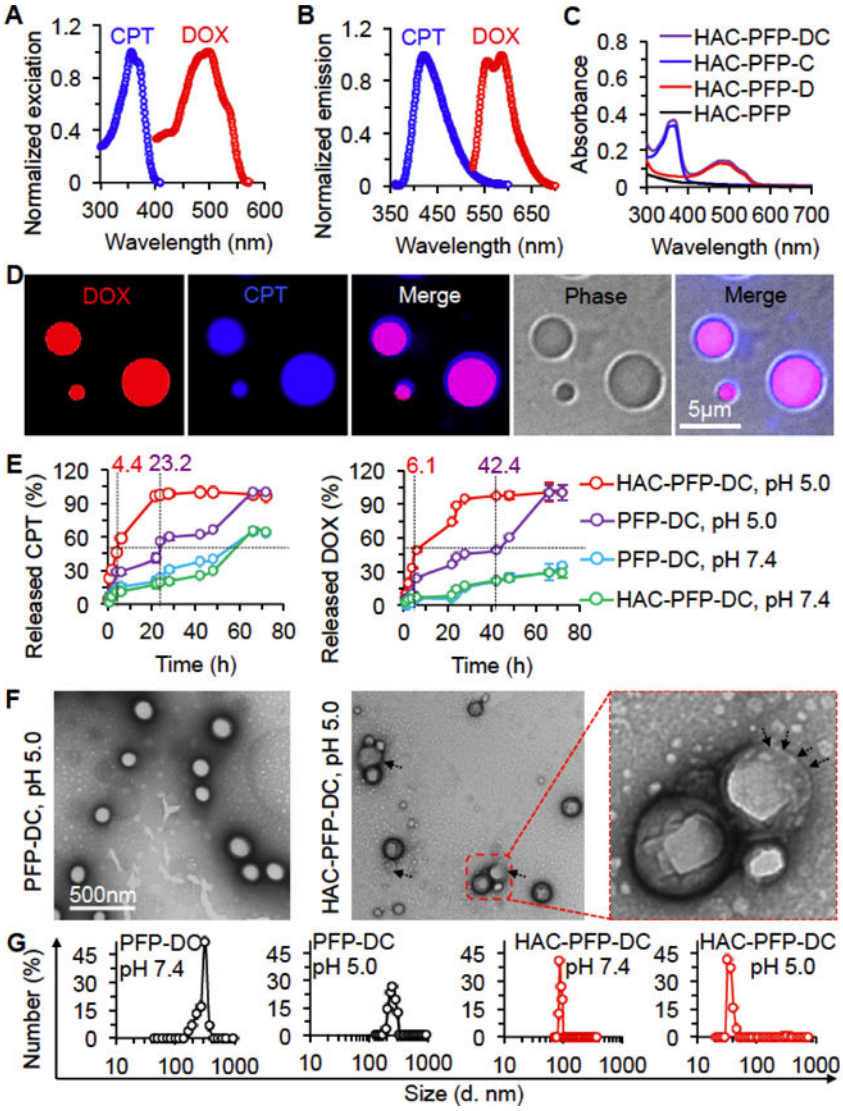

Fig. 3.

Characterization of drug encapsulation and release showing the acidic pH-triggered drug release from the HAC-PFP-DC nanoparticles. Normalized excitation (A) and fluorescence emission (B) spectra of HAC-PFP-DC nanoparticles showing the presence of both DOX and CPT in the nanoparticles. (C) UV-Vis absorbance of HAC-PFP-DC nanoparticles showing the presence of both DOX and CPT in the nanoparticles. (D) Fluorescence images of the HAC-PFP-DC nanoparticles before rotary evaporation to remove organic solvent showing that both DOX (red) and CPT (blue) existed in each particle. (E) *In vitro* release of CPT and DOX from PFP-DC and HAC-PFP-DC nanoparticles at pH 5.0 and 7.4 showing the acidic pH-triggered drug release from both (particularly the HAC-PFP-DC) nanoparticles. TEM images (F) and DLS data (G) of PFP-DC and HAC-PFP-DC nanoparticles after incubated at pH 7.4 and 5 at 37 °C for 3 h. The arrows in the TEM images of HAC-PFP-DC nanoparticles indicate compromised nanoparticles.

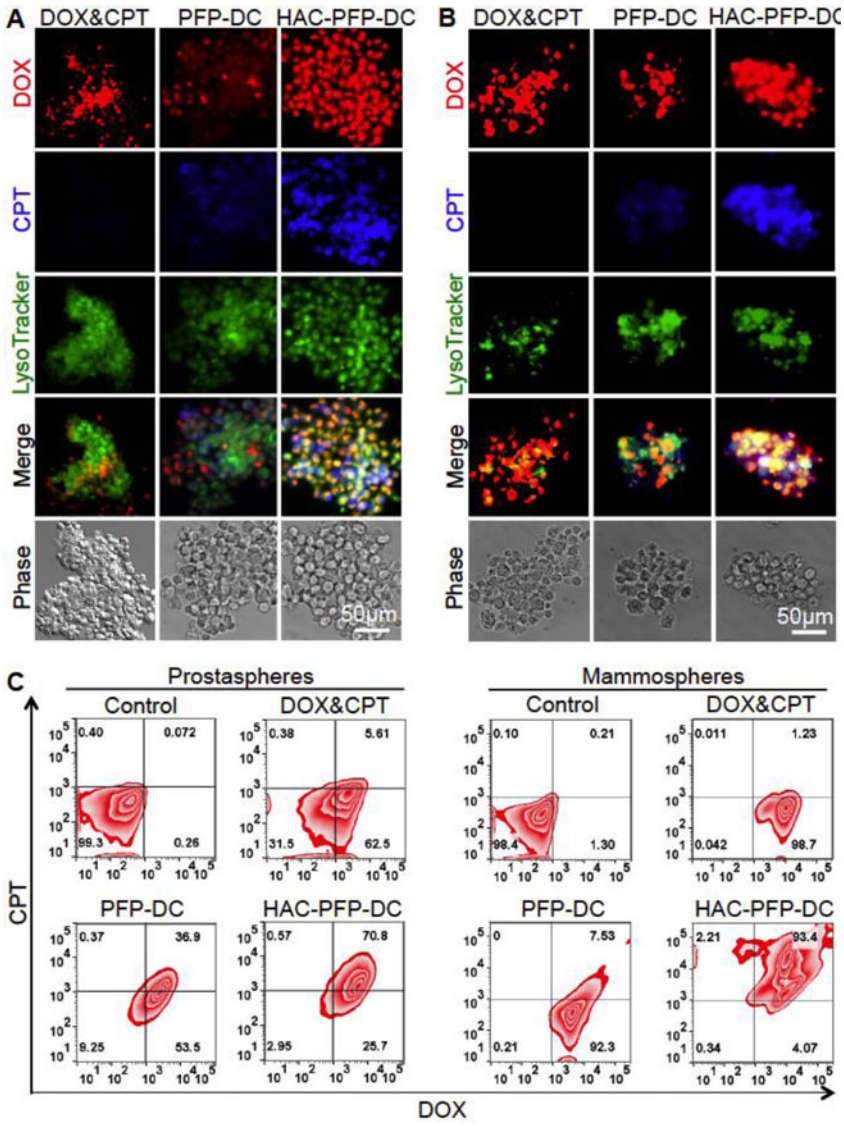

Fig. 4.

In vitro cell uptake data showing the HA coating on HAC-PFP-DC nanoparticles significantly improves drug delivery into prostasphere and mammosphere cells enriched with CSCs. Fluorescence micrographs of (A) prostasphere and (B) mammosphere cells after incubated with the simple mixture of free DOX&CPT, PFP-DC nanoparticles, and HAC-PFP-DC nanoparticles for 3 h at 37 °C. (C) Typical flow cytometry data of fluorescence intensity of DOX and CPT in both prostasphere and mammosphere cells after the three different treatments. Collectively, the data show enhanced cellular uptake of both anticancer drugs delivered using HA-PPF-DC nanoparticles via endocytosis by both mammosphere and prostasphere cells, compared to PFP-DC nanoparticles and free anticancer drugs. The LysoTracker green stains late endosomes and lysosomes.

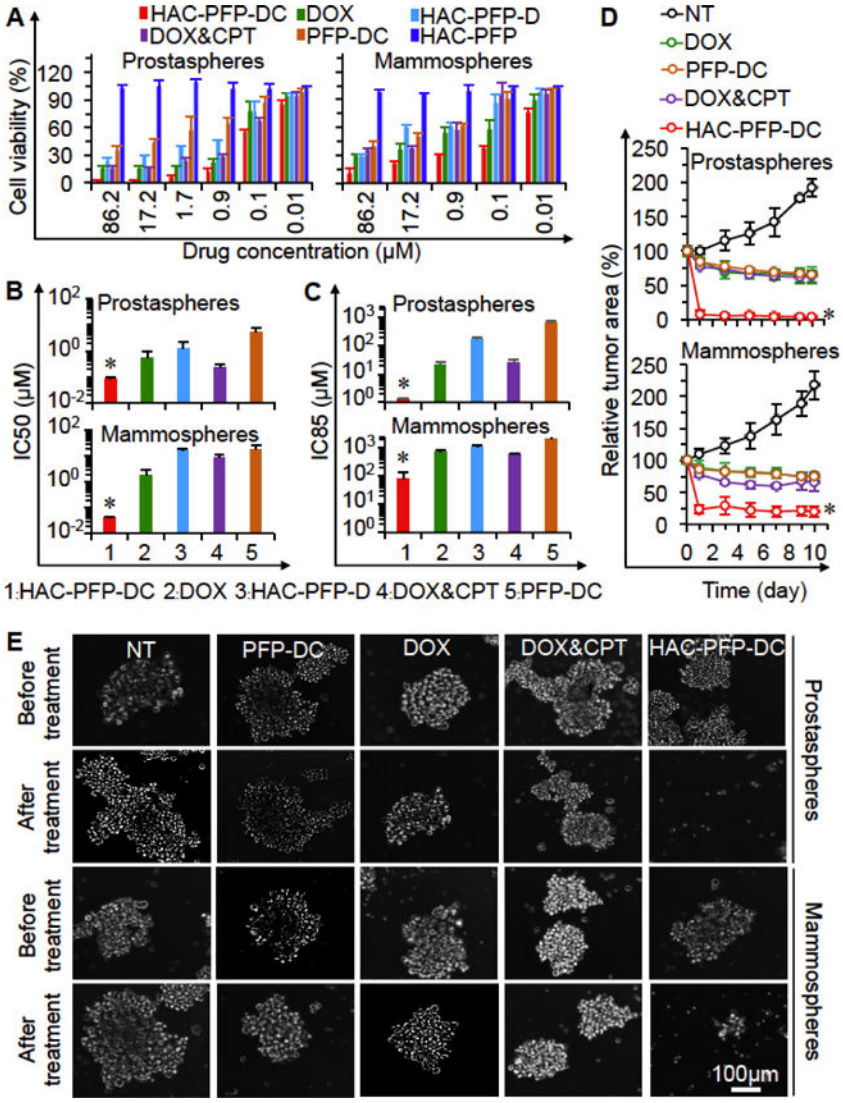

Fig. 5.

The HAC-PFP-DC nanoparticles exhibit excellent anti-CSC capability *in vitro*. (A) Viability of prostasphere and mammosphere cells after treated with free DOX, simple mixture of free DOX&CPT, PFP-DC nanoparticles, HAC-PFP-D nanoparticles, and HAC-PFP-DC nanoparticles. (B) IC50 (inhibitory concentration to kill 50% cells) and (C) IC85 (inhibitory concentration to kill 85% cells) calculated from the viability data for the various drug formulations. (D) Growth (area normalized to that of the first day) curve of prostaspheres and mammospheres after treated with 1.72 μM drug in various formulations together with no treatment (NT) control. (E) Typical micrographs showing morphology of the prostasphere and mammospheres after treated with 1.72 μM drug in various formulations for 10 days together with no treatment (NT) control. *: $p < 0.05$.

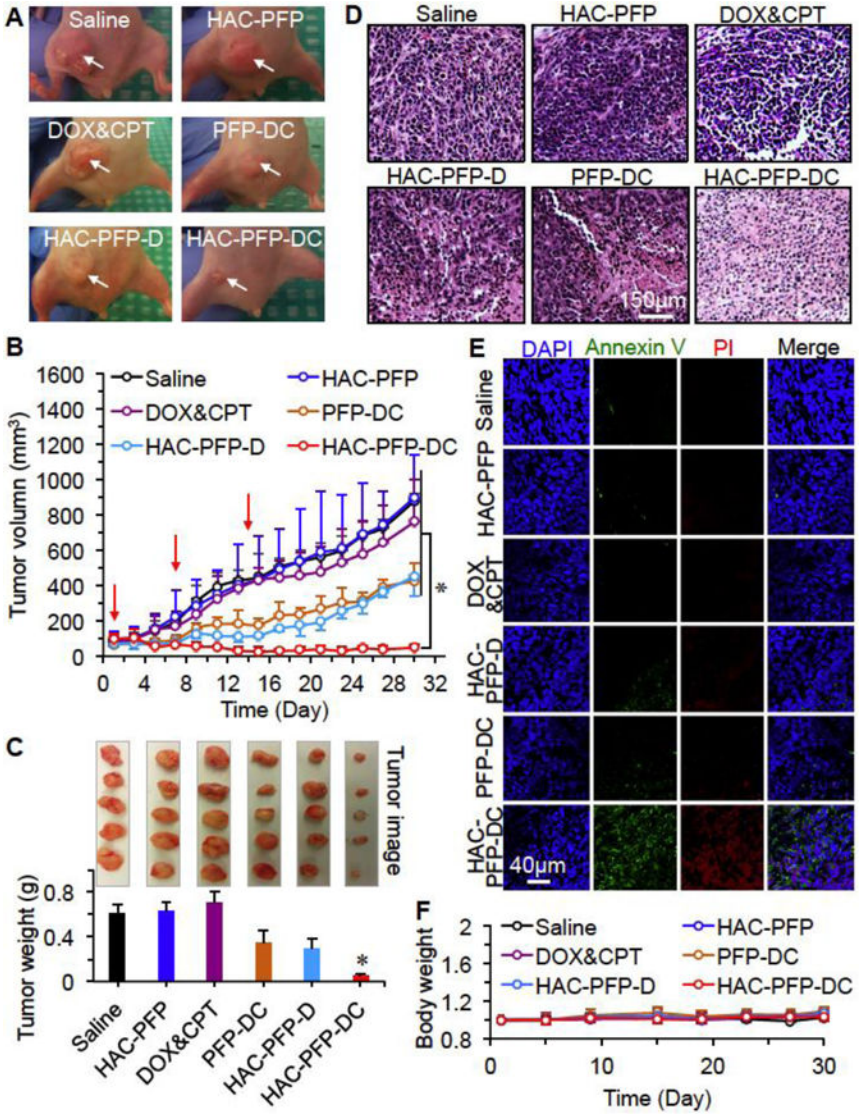

Fig. 6.

The HAC-PFP-DC nanoparticles exhibit excellent *in vivo* anti-tumor capacity. (A) Typical photographs showing the size of tumors (indicated by arrows) in mice on day 30 after six different treatments. (B) Tumor growth curves for various drug formulation treatments. *: $p < 0.05$. (C) Weight of the tumors together with images of tumors collected after sacrificing the mice on day 30. *: $p < 0.05$. (D) Representative histology (H&E) images of the tumors collected on day 30. (E) Staining of early and late apoptosis of cells in the tumors collected on day 30 with Annexin V and PI, respectively. The DAPI stains cell nuclei. (F) Relative (to saline control) body weight of the mice with the various treatments showing no significant difference between the different treatments.

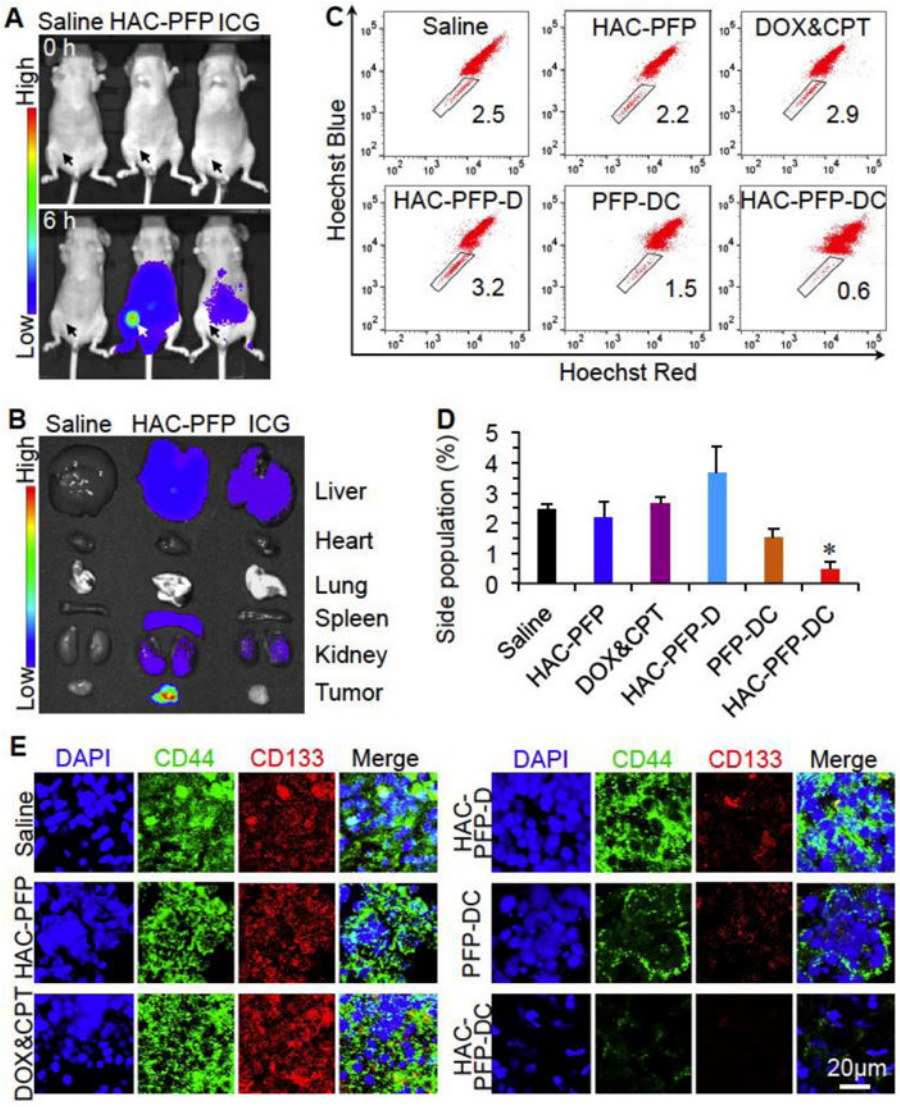

Fig. 7.

The HAC-PFP-DC nanoparticles target tumors and effectively kill CSCs *in vivo*. (A) *In vivo* whole animal imaging of ICG fluorescence at 6 h after intravenous injection via the tail vein in the forms of free ICG and ICG-laden HAC-PFP nanoparticles. The arrows indicate the locations of tumors in mice. (B) *Ex vivo* imaging of ICG fluorescence in tumor and five important organs collected after sacrificing the mice at 6 h. (C) Typical 2-channel flow cytometry data showing the distinct side population that excludes Hoechst 33342 stain in tumor cells obtained after sacrificing the mice on day 30 with different treatments. (D) The corresponding quantitative percentage data of the side population. *: $p < 0.05$. (E) Immunohistochemical staining of CD44 and CD133 in tumor showing diminished expression of both CD44 and CD133 after the treatment with HAC-PFP-DC nanoparticles. ICG: indocyanine green.